

Dark matter in $U(1)$ extensions of the MSSM with gauge kinetic mixing

Geneviève Bélanger^{a,1}, Jonathan Da Silva^{b,2} and Hieu Minh Tran^{c,3}

^a*LAPTH, Université Savoie Mont Blanc, CNRS, B.P.110, F74941 Annecy Cedex, France*

^b*Laboratoire de Physique Subatomique et de Cosmologie, Université Grenoble-Alpes, CNRS/IN2P3, 53 Avenue Des Martyrs, F-38026 Grenoble, France*

^c*Hanoi University of Science and Technology, 1 Dai Co Viet Road, Hanoi, Vietnam*

Abstract

The gauge kinetic mixing in general is allowed in models with multiple Abelian gauge groups. In this paper, we investigate the gauge kinetic mixing in the framework of $U(1)$ extensions of the MSSM. It enlarges the viable parameter space, and has an important effect on the particle mass spectrum as well as the Z_2 coupling with matters. The SM-like Higgs boson mass can be enhanced with a nonzero kinetic mixing parameter and the muon $g - 2$ tension is slightly less severe than in the case of no mixing. We present the results from both benchmark analysis and global parameter scan. Various theoretical and phenomenological constraints have been considered. The recent LHC searches for the Z_2 boson are important for the case of large positive kinetic mixing where the Z_2 coupling is enhanced, and severely constrain scenarios with $M_{Z_2} < 2.8$ TeV. The viable dark matter candidate predicted by the model is either the neutralino or the right-handed sneutrino. Cosmological constraints from dark matter searches play a significant role in excluding the parameter space. Portions of the parameter space with relatively low sparticle mass spectrum can be successfully explored in the LHC run-2 as well as future linear colliders and dark matter searches.

¹ E-mail: belanger@lapth.cnrs.fr

² E-mail: jonathan.da.silva.physics@gmail.com

³ E-mail: hieu.tranminh@hust.edu.vn

1 Introduction

Although the standard model (SM) has been verified to a very high accuracy, an extension is necessary both for theoretical consistency and in order to explain experimental observations. The minimal supersymmetric (SUSY) extension of the SM (MSSM) has played an important role in phenomenological studies for many years because it could address many fundamental issues such as the gauge hierarchy problem, the prediction of the Higgs boson mass, and the gauge coupling unification while also providing a dark matter (DM) candidate, the lightest neutralino. Nevertheless, the discovery of a 125 GeV Higgs boson [1, 2] has imposed some tension on the MSSM. In order to reconcile the Higgs boson mass, large loop corrections are needed, these in general require heavy squarks (especially stops) and a large mixing, thus reintroducing a certain amount of fine-tuning to the theory [3]. Moreover, the parameter regions with maximal stop mixing which allow to obtain the observed Higgs mass potentially have a metastable electroweak vacuum, and predict a global minimum which breaks charge and/or color symmetries [4–6]. In scenarios where the number of free parameters is limited due to some relations at a high energy scale, heavy squarks imply heavy sleptons [7, 8]. Hence, the SUSY contribution to the muon anomalous magnetic dipole moment ($g - 2$) can hardly explain the discrepancy between the SM prediction and the experimental result. This last issue is however easily resolved when allowing a larger hierarchy between the slepton and squark masses.

There have been attempts to resolve these tensions, see for example [9–11] and references therein. In this paper, we consider $U(1)'$ extensions of the MSSM (UMSSM) that can also improve the situation [12–16]. The interaction between the extra singlet superfield, whose vacuum expectation value (VEV) breaks the $U(1)'$, and the two Higgs doublets helps to increase the mass of the SM-like Higgs at the tree level. This contribution is the same as in the next-to-MSSM (NMSSM) [17–20]. In addition, the SM-like Higgs boson mass is also enhanced by the $U(1)'$ D-term contribution [21, 22]. Both these effects imply that the loop-induced contribution from the stop sector does not need to be large. In this framework, as in the NMSSM, the μ -term problem is solved since this term is not introduced by hand but is generated by the vacuum expectation value of the singlet after the extra gauge group $U(1)'$ is broken. The physics origin of the $U(1)'$ group depends on the specific scenario, for instance $U(1)_{B-L}$, or inherited from some grand unified theory (GUT). Here we are interested in the scenario where the $U(1)'$ is a remnant symmetry after the breaking of the E_6 GUT [23]. This scenario is also motivated by superstring models [24, 25].

To account for the neutrino oscillations, we introduce in the model three generations of right-handed (RH) neutrinos. Assuming R-parity conservation, their superpartners which are

weakly interacting massive particles can play the role of DM. This is in contrast with left-handed (LH) sneutrinos, which although also weakly interacting, have been ruled out as a DM candidate because their scattering cross section onto nuclei is too large [26]. This model offers two possible candidates for the DM, the ordinary neutralino and the right handed sneutrino, depending on which one is the lightest superparticle (LSP).

A special feature of models with two Abelian gauge groups $U(1) \times U(1)'$, is that a gauge kinetic mixing term can exist in the Lagrangian without violating any underlying symmetry [27–30]:

$$\mathcal{L} \supset -\frac{k}{2} F^{\mu\nu} F'_{\nu\mu}. \quad (1)$$

Generally, even in the case that the kinetic mixing term is set to zero at some scale, it can be radiatively generated at the low energy scale due to the renormalization group (RG) evolution [31,32]. It was found that in the $U(1)_{B-L}$ case the gauge kinetic mixing effect can be significant and impact DM observables [33,34,36].

DM properties in $U(1)$ extensions of the MSSM were examined in [15,37–39] and the compatibility of the UMSSM with collider and DM observables was examined in [16] where the kinetic mixing was neglected. Here we revisit and update the constraints on the parameter space of the UMSSM inspired from E_6 GUT, while including the kinetic mixing. The radiatively generated kinetic mixing term depends on the particle content and the charge assignment of fields under the two $U(1)$ gauge groups. For example, in the minimal SUSY $B - L$ model [34] the kinetic mixing parameter purely induced from the RG evolution is positive and sizable, $k \sim \mathcal{O}(1)$, while in E_6 models [35] the value of k at low energies can be either positive or negative. To be completely general, we will consider that k is a free parameter set at the low energy scale.

We will show that the gauge kinetic mixing can give rise to important effects on both the mass spectrum and DM properties. For example the kinetic mixing allows for a leptophobic Z_2 which can more easily escape LHC constraints, gives a contribution to the mass of the Higgs boson, can shift the mass of sleptons thus providing a better agreement with the muon anomalous magnetic moment, and finally impact the DM annihilation channel. Note that in this study we include updated constraints from the LHC searches on a heavy neutral gauge boson Z_2 as well as updated constraints from DM direct detection from LUX [40].

The structure of the paper is as follows. In Section 2, we briefly describe the UMSSM model with gauge kinetic mixing. The effects of the kinetic mixing term on the parameter space, the Z_2 coupling with matter, and the mass spectrum are shown in Section 3. Here, benchmark analysis and results of the global parameter scan are presented with various collider constraints as well as cosmological ones taken into account. Section 4 is devoted for conclusion.

	Q	U^c	D^c	L	N^c	E^c	H_u	H_d	S
$\sqrt{40}\mathcal{Q}'_\chi$	-1	-1	3	3	-5	-1	2	-2	0
$\sqrt{24}\mathcal{Q}'_\psi$	1	1	1	1	1	1	-2	-2	4

Table 1: $U(1)'$ charges of chiral superfields.

2 The UMSSM with gauge kinetic mixing

2.1 The model

The UMSSM has the gauge groups $SU(3)_C \times SU(2)_L \times U(1)_Y \times U(1)'$ which remain after the symmetry breaking of an E_6 GUT. The particle contents of this model include the MSSM chiral supermultiplets, three generations of RH neutrino supermultiplets $N^c = \{\tilde{\nu}_R^c, \nu_R^c\}$, the MSSM vector supermultiplets and an additional vector supermultiplet $V' = \{\tilde{B}', B'_\mu\}$ corresponding to $U(1)'$ gauge group, and a Higgs singlet superfield S responsible for the $U(1)'$ breaking. Additional chiral supermultiplets are included in an anomaly free E_6 theory. For simplicity, we assume that all the fields belong to the **27** representations of E_6 that are not listed above are heavy enough to be safely neglected at low energies.

The $U(1)'$ charge of a chiral superfields is given by

$$\mathcal{Q}' = \cos \theta_{E_6} \mathcal{Q}'_\chi + \sin \theta_{E_6} \mathcal{Q}'_\psi, \quad (2)$$

where $\theta_{E_6} \in [-\frac{\pi}{2}, \frac{\pi}{2}]$ parameterizes a linear combination of two E_6 subgroups $U(1)_\chi$ and $U(1)_\psi$ into $U(1)'$. The charges \mathcal{Q}'_χ and \mathcal{Q}'_ψ for each chiral superfield of the model are given in Table 1.

The superpotential of the model involves the ordinary MSSM superpotential without the μ -term, and other terms describing interactions of the Higgs singlet and right handed neutrinos:

$$\mathcal{W} \supset \mathcal{W}_{\text{MSSM}}|_{\mu=0} + \lambda S H_u H_d + N^c \mathbf{Y}_\nu L H_u, \quad (3)$$

where \mathbf{Y}_ν is the neutrino Yukawa coupling matrix responsible for the neutrino mass generation. After the $U(1)'$ group is broken, the μ -term is generated by the singlet's VEV, $\langle S \rangle = \frac{v_S}{\sqrt{2}}$ as

$$\mu = \lambda \frac{v_S}{\sqrt{2}}. \quad (4)$$

The soft SUSY breaking Lagrangian of the UMSSM reads

$$\begin{aligned} \mathcal{L}^{\text{soft}} \supset & \mathcal{L}_{\text{MSSM}}^{\text{soft}}|_{B_\mu=0} - \left(\frac{1}{2} M'_1 \tilde{B}' \tilde{B}' + \tilde{\nu}_R^c \mathbf{A}_\nu \tilde{L} H_u + h.c. \right) - \tilde{\nu}_R^c \mathbf{M}_{\tilde{\nu}_R}^2 \tilde{\nu}_R \\ & - m_S^2 |S|^2 - (\lambda A_\lambda S H_u H_d + h.c.), \end{aligned} \quad (5)$$

where new soft terms are added in comparison to the MSSM: the \tilde{B}' soft mass, M'_1 , the neutrino trilinear couplings, \mathbf{A}_ν , the right handed sneutrinos soft masses, $\mathbf{M}_{\tilde{\nu}_R}^2$, the singlino mass, m_S , and the Higgs trilinear coupling, A_λ . Similar to Eq. (4), the MSSM $B\mu$ term is induced by the $U(1)'$ breaking:

$$B\mu = \lambda A_\lambda \frac{v_S}{\sqrt{2}}. \quad (6)$$

2.2 Gauge kinetic mixing

The general gauge kinetic Lagrangian for Abelian gauge superfields is written as follows

$$\mathcal{L}_{\text{kinetic}}^{\text{gauge}} \supset - \int d^4\theta \frac{1}{4} \begin{pmatrix} W^\alpha & W'^\alpha \end{pmatrix} \begin{pmatrix} 1 & k \\ k & 1 \end{pmatrix} \begin{pmatrix} W_\alpha \\ W'_\alpha \end{pmatrix} + h.c., \quad (7)$$

where the off-diagonal element k is the gauge kinetic mixing parameter. The kinetic mixing matrix can be diagonalized by a rotation among the original Abelian vector superfields, (\hat{V}, \hat{V}') :

$$\begin{pmatrix} \hat{V} \\ \hat{V}' \end{pmatrix} = \begin{pmatrix} \frac{1}{\sqrt{2(1+k)}} & \frac{-1}{\sqrt{2(1-k)}} \\ \frac{1}{\sqrt{2(1+k)}} & \frac{1}{\sqrt{2(1-k)}} \end{pmatrix} \begin{pmatrix} V_Y \\ V_E \end{pmatrix}. \quad (8)$$

For a real rotation, the kinetic mixing parameter is limited to $-1 < k < 1$. The rotation (8) ensures that there is no explicit kinetic mixing in the Lagrangian written in the new basis (V_Y, V_E) . However, the effect of the kinetic mixing term now transfers to the interactions between the Abelian vector superfields and chiral superfields. The gauge interaction Lagrangian is

$$\mathcal{L}_{\text{interaction}}^{\text{gauge}} \supset \int d^4\theta \Phi^\dagger e^{\mathbf{Q} \cdot \mathbf{g} \cdot \mathbf{V}} \Phi, \quad (9)$$

where

$$\mathbf{Q} \cdot \mathbf{g} \cdot \mathbf{V} = \begin{pmatrix} Y & \mathcal{Q}' \end{pmatrix} \begin{pmatrix} g_{YY} & g_{YE} \\ g_{EY} & g_{EE} \end{pmatrix} \begin{pmatrix} V_Y \\ V_E \end{pmatrix}. \quad (10)$$

where Y is the hypercharge and \mathcal{Q}' the charge associated with $U(1)'$. The gauge coupling matrix which is originally diagonal absorbs the rotation of the Abelian vector superfields, and becomes non-diagonal:⁴

$$\begin{pmatrix} g_{YY} & g_{YE} \\ g_{EY} & g_{EE} \end{pmatrix} = \begin{pmatrix} \frac{g_1}{\sqrt{2(1+k)}} & \frac{-g_1}{\sqrt{2(1-k)}} \\ \frac{g'_1}{\sqrt{2(1+k)}} & \frac{g'_1}{\sqrt{2(1-k)}} \end{pmatrix}. \quad (11)$$

⁴ In our analysis in the next section, we will assume for simplicity that $g'_1 = \sqrt{\frac{5}{3}}g_1$.

To simplify the gauge coupling matrix, we perform an orthogonal rotation in the space of Abelian vector superfields such that the gauge kinetic matrix remains intact:

$$\begin{pmatrix} V_Y \\ V_E \end{pmatrix} = \frac{1}{\sqrt{g_{EE}^2 + g_{EY}^2}} \begin{pmatrix} g_{EE} & g_{EY} \\ -g_{EY} & g_{EE} \end{pmatrix} \begin{pmatrix} V \\ V' \end{pmatrix}. \quad (12)$$

Eq. (10) is then rewritten as

$$\mathbf{Q} \cdot \mathbf{g} \cdot \mathbf{V} = \begin{pmatrix} Y & \mathcal{Q}' \end{pmatrix} \begin{pmatrix} g_y & g' \\ 0 & g_E \end{pmatrix} \begin{pmatrix} V \\ V' \end{pmatrix}, \quad (13)$$

in which

$$g_y = \frac{g_{YY}g_{EE} - g_{YE}g_{EY}}{\sqrt{g_{EE}^2 + g_{EY}^2}} = g_1, \quad (14)$$

$$g' = \frac{g_{YY}g_{EY} + g_{YE}g_{EE}}{\sqrt{g_{EE}^2 + g_{EY}^2}} = \frac{-kg_1}{\sqrt{1 - k^2}}, \quad (15)$$

$$g_E = \frac{\sqrt{g_{EE}^2 + g_{EY}^2}}{\sqrt{1 - k^2}} = \frac{g'_1}{\sqrt{1 - k^2}}. \quad (16)$$

Note that in the limit $k \rightarrow 0$, the above Abelian gauge coupling matrix becomes diagonal. Performing matrix multiplication in Eq. 13, we obtain:

$$\mathbf{Q} \cdot \mathbf{g} \cdot \mathbf{V} = Yg_1V + Q^p g_E V', \quad (17)$$

where the new charge Q^p is defined as

$$Q^p = \mathcal{Q}' - k \frac{g_1}{g'_1} Y. \quad (18)$$

Clearly, Y corresponds to the SM hypercharge and V is the associated gauge superfield while the kinetic mixing induces a shift in the new charge of the chiral superfields, from $\mathcal{Q}' \rightarrow Q^p$, and the coupling with the new Abelian superfield, from $g'_1 \rightarrow g_E$. It is worth to note that the anomaly cancellation conditions for $\{\mathcal{Q}', Y\}$ in the underlying E_6 theory ensure the theory to be anomaly free for the redefined charge Q^p .

2.3 Neutral gauge bosons

The original Abelian vector superfields (\hat{V}, \hat{V}') are mixed to form the new ones (V, V') . Their vector components (B_μ, B'_μ) in turn mix with the third component W_μ^3 of the $SU(2)_L$ gauge group to form mass eigenstates $(A_\mu, Z_{1\mu}, Z_{2\mu})$ when the gauge groups $SU(2)_L \times U(1)_Y \times U(1)'$ are broken spontaneously. The Z -boson mixing mass matrix is as follows

$$\mathbf{M}_Z^2 = \begin{pmatrix} M_{ZZ}^2 & M_{ZZ'}^2 \\ M_{ZZ'}^2 & M_{Z'Z'}^2 \end{pmatrix}, \quad (19)$$

where

$$\begin{aligned}
M_{ZZ}^2 &= \frac{1}{4}g_1^2(v_u^2 + v_d^2), \\
M_{Z'Z'}^2 &= g_E^2 [(Q_{H_u}^p)^2 v_u^2 + (Q_{H_d}^p)^2 v_d^2 + (Q_S^p)^2 v_S^2], \\
M_{ZZ'}^2 &= \frac{1}{2}g_1 g_E (Q_{H_u}^p v_u^2 - Q_{H_d}^p v_d^2).
\end{aligned} \tag{20}$$

This matrix can be diagonalized by an orthogonal rotation:

$$\begin{pmatrix} Z_1 \\ Z_2 \end{pmatrix} = \begin{pmatrix} \cos \alpha_Z & \sin \alpha_Z \\ -\sin \alpha_Z & \cos \alpha_Z \end{pmatrix} \begin{pmatrix} Z^0 \\ Z' \end{pmatrix}, \tag{21}$$

where α_Z is the mixing angle defined as

$$\sin 2\alpha_Z = \frac{2M_{ZZ'}^2}{M_{Z_2}^2 - M_{Z_1}^2} \tag{22}$$

The physical states Z_1 and Z_2 have masses:

$$M_{Z_1, Z_2}^2 = \frac{1}{2} \left[M_{ZZ}^2 + M_{Z'Z'}^2 \mp \sqrt{(M_{ZZ}^2 - M_{Z'Z'}^2)^2 + 4M_{ZZ'}^4} \right] \tag{23}$$

In our analysis, we use the measured Z-boson mass for M_{Z_1} , while M_{Z_2} and α_Z are considered as free parameters.

2.4 Sfermions and neutralinos

In the UMSSM, the D-term contributions to sfermion masses play an important role in forming the sparticle mass spectrum. They modify the diagonal components of the usual MSSM sfermion mass matrices as

$$\Delta_{\tilde{f}} = \frac{1}{2}g_E^2 Q_{\tilde{f}}^p (Q_{H_u}^p v_u^2 + Q_{H_d}^p v_d^2 + Q_S^p v_S^2), \tag{24}$$

where $\tilde{f} = \{\tilde{q}_L^i, \tilde{u}_R^i, \tilde{d}_R^i, \tilde{l}_L^i, \tilde{\nu}_R^i, \tilde{e}_R^i\}$ with the generation index $i = \{1, 2, 3\}$. Since the redefined charges Q^p and gauge coupling g_E are functions of k , the sparticle mass spectrum also depends on the kinetic mixing parameter. As we will see, this effect is particularly important.

While charginos are the same as in the MSSM, the neutralino sector of the UMSSM consists of six fermions. Their masses are eigenvalues obtained from the mass matrix that is written in the basis of neutral fermionic components of the vector supermultiplets and the Higgs super-

multiplets $\psi^0 = (\tilde{B}, \tilde{W}^3, \tilde{H}_d, \tilde{H}_u, \tilde{S}, \tilde{B}')^T$ as

$$\mathbf{M}_{\tilde{\chi}^0} = \begin{pmatrix} M_1 & 0 & -M_{ZZc_\beta s_W} & M_{ZZs_\beta s_W} & 0 & 0 \\ 0 & M_2 & M_{ZZc_\beta c_W} & -M_{ZZs_\beta c_W} & 0 & 0 \\ -M_{ZZc_\beta s_W} & M_{ZZc_\beta c_W} & 0 & -\mu & -\lambda \frac{v_u}{\sqrt{2}} & Q_{H_d}^p g_E v_d \\ M_{ZZs_\beta s_W} & -M_{ZZs_\beta c_W} & -\mu & 0 & -\lambda \frac{v_d}{\sqrt{2}} & Q_{H_u}^p g_E v_u \\ 0 & 0 & -\lambda \frac{v_u}{\sqrt{2}} & -\lambda \frac{v_d}{\sqrt{2}} & 0 & Q_S^p g_E v_S \\ 0 & 0 & Q_{H_d}^p g_E v_d & Q_{H_u}^p g_E v_u & Q_S^p g_E v_S & M'_1 \end{pmatrix}, \quad (25)$$

where $c_W = \cos \theta_W$, $s_W = \sin \theta_W$, $c_\beta = \cos \beta$, $s_\beta = \sin \beta$, with $\tan \beta = \frac{v_u}{v_d}$. The value of $\tan \beta$ can be derived using Eqs. (21) and (22). We have

$$\cos^2 \beta = \frac{1}{Q_{H_u}^p + Q_{H_d}^p} \left(\frac{\sin 2\alpha_Z (M_{Z_1}^2 - M_{Z_2}^2)}{v^2 g_E \sqrt{g_1^2 + g_2^2}} + Q_{H_u}^p \right), \quad (26)$$

in which $v^2 = v_u^2 + v_d^2$ and g_2 is the SU(2) coupling. The matrix \mathbf{Z}_n diagonalizing the above mass matrix determines the components of each neutralino:

$$\tilde{\chi}_i^0 = (\mathbf{Z}_n)_{ij} \psi_j^0, \quad i, j = \{1, 2, 3, 4, 5, 6\}, \quad (27)$$

and therefore its properties.

2.5 Higgs sector

The tree level mass-squared matrix of CP-even Higgs bosons is a symmetric 3×3 matrix \mathcal{M}'_+ with elements computed as:

$$\begin{aligned} (\mathcal{M}'_+)_{11} &= \left[\frac{g_1^2 + g_2^2}{4} + (Q_{H_d}^p)^2 g_E^2 \right] v_d^2 + \frac{\lambda A_\lambda v_S v_u}{\sqrt{2} v_d}, \\ (\mathcal{M}'_+)_{12} &= - \left[\frac{g_1^2 + g_2^2}{4} - \lambda^2 - Q_{H_u}^p Q_{H_d}^p g_E^2 \right] v_u v_d - \frac{\lambda A_\lambda v_S}{\sqrt{2}}, \\ (\mathcal{M}'_+)_{13} &= [\lambda^2 + Q_{H_d}^p Q_S^p g_E^2] v_S v_d - \frac{\lambda A_\lambda v_u}{\sqrt{2}}, \\ (\mathcal{M}'_+)_{22} &= \left[\frac{g_1^2 + g_2^2}{4} + (Q_{H_u}^p)^2 g_E^2 \right] v_u^2 + \frac{\lambda A_\lambda v_S v_d}{\sqrt{2} v_u}, \\ (\mathcal{M}'_+)_{23} &= [\lambda^2 + Q_{H_u}^p Q_S^p g_E^2] v_S v_u - \frac{\lambda A_\lambda v_d}{\sqrt{2}}, \\ (\mathcal{M}'_+)_{33} &= (Q_S^p)^2 g_E^2 v_S^2 + \frac{\lambda A_\lambda v_u v_d}{\sqrt{2} v_S}. \end{aligned} \quad (28)$$

The lightest Higgs boson is the SM-like one. Its tree level mass can be written approximately as [41]

$$m_{h_1}^2|_{\text{tree}} \simeq M_{ZZ}^2 \cos^2 2\beta + \frac{1}{2}\lambda^2 v^2 \sin^2 2\beta + g_E^2 v^2 (Q_{H_d}^p \cos^2 \beta + Q_{H_u}^p \sin^2 \beta)^2 - \frac{\lambda^4 v^2}{g_E^2 (Q_S^p)^2} \left[1 - \frac{A_\lambda \sin^2 2\beta}{2\mu} + \frac{g_E^2}{\lambda^2} (Q_{H_d}^p \cos^2 \beta + Q_{H_u}^p \sin^2 \beta) Q_S^p \right]^2. \quad (29)$$

While the second term in the above equation is the same as in the NMSSM, the last two terms only appear in the UMSSM due to the existence of Q^p and g_E related to the extra $U(1)'$. Therefore the Higgs boson mass depends on the kinetic mixing parameter via these terms. Similarly the masses of h_2 and h_3 can receive large corrections due to the kinetic mixing. There is one CP-odd Higgs A^0 with the mass:

$$m_{A^0}^2|_{\text{tree}} = \frac{\lambda A_\lambda \sqrt{2}}{\sin 2\beta} v_S \left(1 + \frac{v^2}{4v_S^2} \sin^2 2\beta \right). \quad (30)$$

The mass of the charged Higgs bosons is given by

$$m_{H^\pm}^2|_{\text{tree}} = M_W^2 + \frac{\sqrt{2}\lambda A_\lambda}{\sin 2\beta} v_S - \frac{\lambda^2}{2} v^2. \quad (31)$$

These masses also depend on k through the angle β , see Eq. 26.

3 Analysis

3.1 Theoretical constraints

In Eq. (17), we have interpreted g_E as a redefined $U(1)'$ gauge coupling. It is crucial to check under which condition this new coupling satisfies the perturbation limit:

$$\alpha_E = \frac{g_E(k)^2}{4\pi} \lesssim 1. \quad (32)$$

Replacing with the coupling definition in Eq. 16, this condition leads to an upper bound on $k^2 < 1 - g_1'^2/4\pi$. This constraint is weak and only excludes the regions of k close to ± 1 .

In this model, $\tan \beta$ is not chosen as an independent parameter as in the MSSM. It depends on the values of four other free parameters M_{Z_2} , α_Z , θ_{E_6} , and the kinetic mixing k as expressed in Eq. (26). The reality condition on the angle β ,

$$0 \leq \cos^2 \beta \leq 1, \quad (33)$$

defines the regions in the parameter space of $\{M_{Z_2}, \alpha_Z, \theta_{E_6}, k\}$ where further calculations can be carried out. In Figs 1, 2 and 3, we show the parameter regions allowed by the constraint

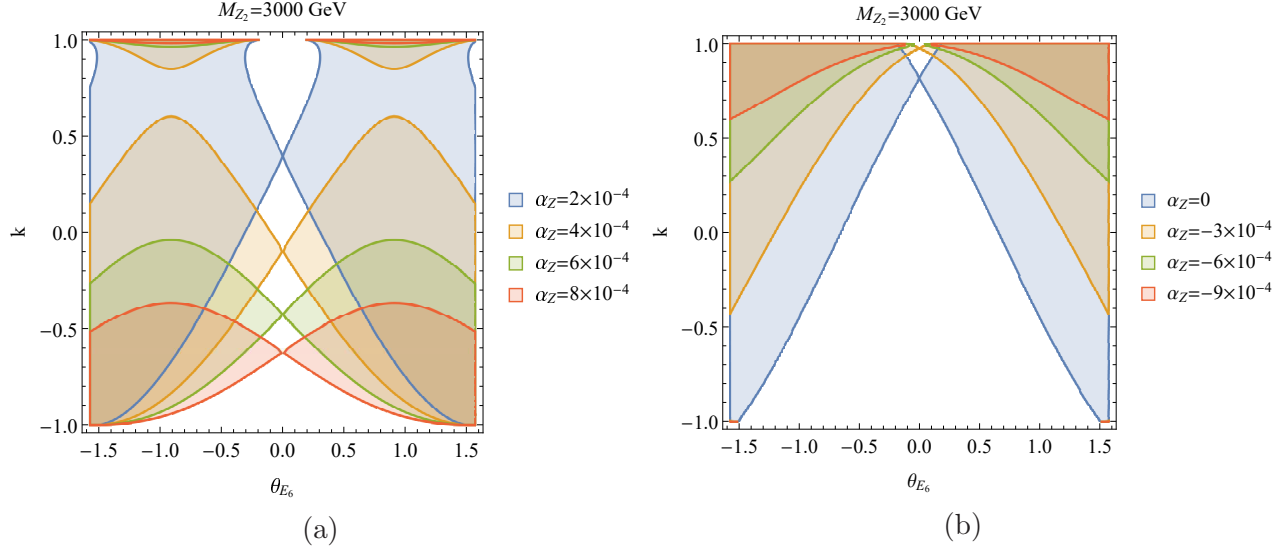


Figure 1: Allowed regions in the (θ_{E_6}, k) plane for the case of the Z_2 boson mass $M_{Z_2} = 3000$ GeV and various values of the angle α_Z : (1a) $\alpha_Z > 0$, (1b) $\alpha_Z \leq 0$.

(33). For a specific choice of $\{\theta_{E_6}, \alpha_Z, M_{Z_2}\}$, the kinetic mixing parameter k is limited to a specific range that is usually smaller than the open range $(-1, 1)$. Thus by allowing a nonzero kinetic mixing term, the acceptable ranges for other parameters change significantly.

First note that $Q_{H_u}^p + Q_{H_d}^p = -\frac{4}{\sqrt{24}} \sin \theta_{E_6}$. Thus at $\theta_{E_6} = 0$, there is a unique value of k that satisfies Eq. 26 for each choice of $M_{Z'}$ and α_Z . This can be seen in Fig. 1 where the allowed parameter regions in the plane (θ_{E_6}, k) for the case of $M_{Z_2} = 3000$ GeV are depicted. Moreover this value of k is large and positive for $\alpha_Z < 0$, Fig. 1b. Given a choice of (M_{Z_2}, α_Z) , for larger values of θ_{E_6} the range of allowed values for k increases. The sign of k is generally anticorrelated with that of α_Z for large values of the mixing to allow for a cancellation between the two terms in Eq. 26, except when $k \sim +1$. Moreover $|k|$ approaches 1 as the $Z - Z'$ mixing increases. Note that for all cases where the first term in Eq. 26 dominates, the allowed regions are symmetric with respect to a sign flip of θ_{E_6} .

In Fig. 2, we plot the allowed regions in the plane (M_{Z_2}, k) for various values of α_Z and two choices of θ_{E_6} . In the limit of no $Z - Z'$ mixing, $\alpha_Z \approx 0$, the range of values of k become independent of M_{Z_2} and are only set by the conditions $Q_{H_d}^p, Q_{H_u}^p < 0$ for $\theta_{E_6} > 0$, and $Q_{H_d}^p, Q_{H_u}^p > 0$ for $\theta_{E_6} < 0$. Thus the non-zero kinetic mixing implies that regions of parameter space with small values of θ_{E_6} and small mixing α_Z are accessible while they were not with $k = 0$ [16]. However phenomenological constraints that will be discussed in the next section further restrict this region. For non-zero mixing angles, α_Z , larger values of $|k|$ are required to increase g_E and compensate an increase in M_{Z_2} in the first term in Eq. 26. Note that the allowed range for k is quite narrow at large values of M_{Z_2} and that the allowed regions in the

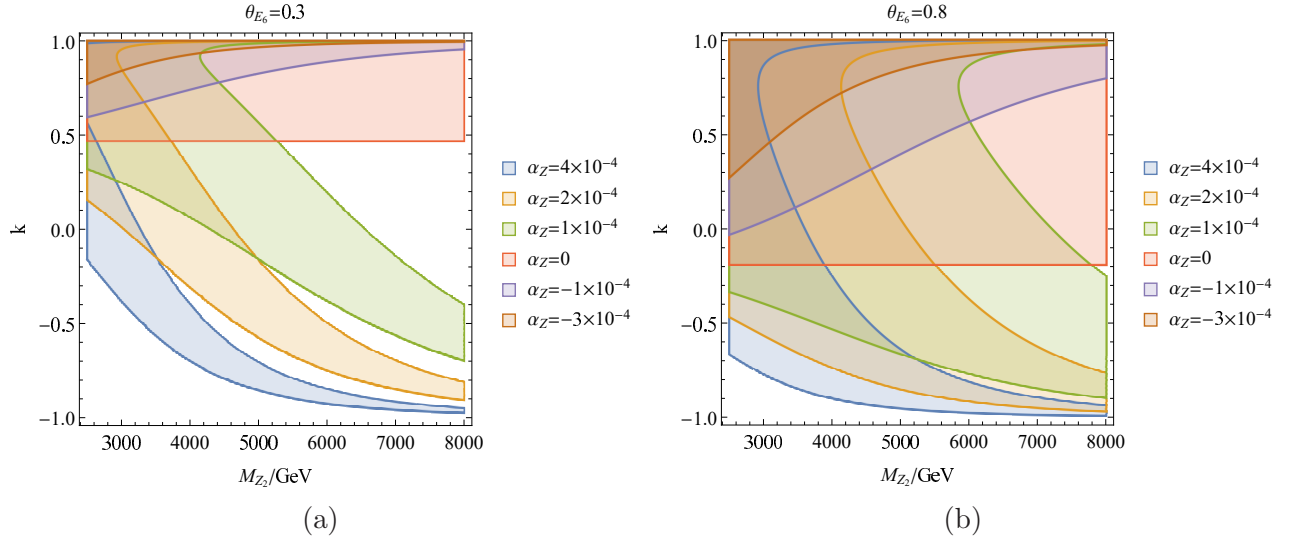


Figure 2: Allowed regions in the (M_{Z_2}, k) plane for various values of α_Z . The angle θ_{E_6} is set to 0.3 and 0.8 in (2a) and (2b) respectively.

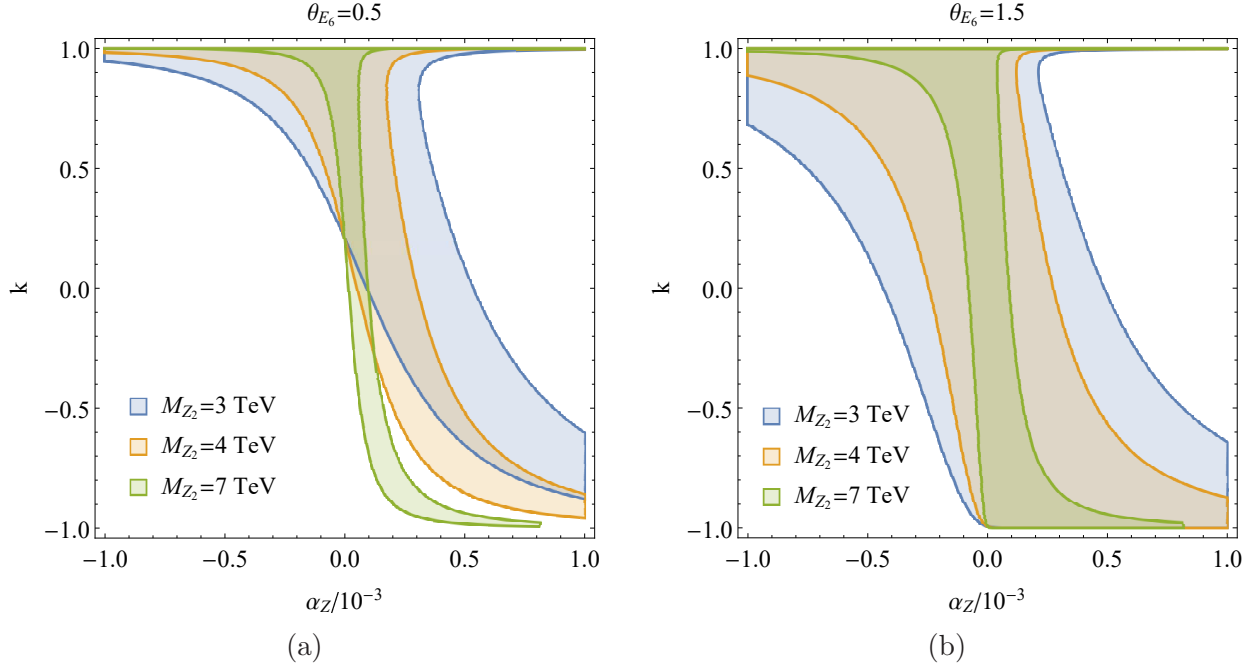


Figure 3: Allowed regions in the (α_Z, k) plane for various values of the Z_2 boson mass M_{Z_2} . The angle θ_{E_6} is chosen to be 0.5 and 1.5 in (3a) and (3b) respectively.

plane (M_{Z_2}, k) become much larger for $\theta_{E_6} = 0.8$ than for $\theta_{E_6} = 0.3$.

We also show in Fig. 3 the allowed regions in the plane (α_Z, k) for various values of the Z_2 boson mass M_{Z_2} . Figs. 3a and 3b correspond to $\theta_{E_6} = 0.5$ and 1.5 respectively. For $\theta_{E_6} = 0.5$, only a narrow range of $Z - Z'$ mixing angles are allowed for $k \approx 0$, while for $k \approx 1$ any value is allowed. Indeed in this case the first term in Eq. 26 becomes strongly suppressed. As mentioned above, for $\theta_{E_6} \approx \pi/2$, a larger area of parameter space is theoretically consistent.

In summary, the presence of the kinetic mixing enlarges significantly the theoretically allowed regions of parameter space, in particular regions with small values of θ_{E_6} , large mixing α_Z and low Z_2 boson mass. Moreover the large positive kinetic mixing ($k \lesssim +1$) is slightly favoured as compared to large negative ($k \gtrsim -1$) as shown in Figs. 1, 2 and 3.

Besides the above theoretical constraints, we also impose perturbative Yukawa couplings, for this we require the Yukawa couplings to be smaller than $\sqrt{4\pi}$ at the SUSY scale. This constraint excludes the possibilities of very small or large values of $\tan\beta$. We also require that the width to mass ratios of Higgs particles should satisfy $\Gamma_{h_i}/m_{h_i} < 1$.

3.2 Phenomenological constraints

In our analysis, various phenomenological constraints are taken into account. For the Higgs boson mass, the combined result of the ATLAS and CMS measurements is employed [42] with a theoretical uncertainty of about 2 GeV. The deflection $\Delta\rho$ of the electroweak ρ -parameter with respect to 1 is computed and compared to current upper bound [43]. We also consider the constraint on the muon anomalous magnetic moment Δa_μ [44–46]. A variety of constraints from flavor physics are taken into account. Observables in the B -meson sector that are of interest include: the oscillation parameters $\Delta M_s, \Delta M_d$ [47], the branching ratios of the following processes: $B^\pm \rightarrow \tau^\pm \nu_\tau$ [48], $\bar{B}^0 \rightarrow X_s \gamma$ [49], $B_s^0 \rightarrow \mu^+ \mu^-$ [43], $\bar{B}^0 \rightarrow X_s \ell^+ \ell^-$ at low and high dilepton invariant mass [50], $b \rightarrow d \gamma$ [51, 52], $B_d^0 \rightarrow \mu^+ \mu^-$ [47], $B \rightarrow X_s \nu \bar{\nu}$ [53], $B^+ \rightarrow K^+ \nu \bar{\nu}$ [47], $B^0 \rightarrow K^{*0} \nu \bar{\nu}$ [47], and the ratios $R_D = \frac{\text{BR}(B^+ \rightarrow D \tau^+ \nu_\tau)}{\text{BR}(B^+ \rightarrow D \ell^+ \nu_\ell)}$, $R_{D^*} = \frac{\text{BR}(B^+ \rightarrow D^* \tau^+ \nu_\tau)}{\text{BR}(B^+ \rightarrow D^* \ell^+ \nu_\ell)}$ [54]. Observables in the Kaon sector include: the branching ratios of the processes $K^+ \rightarrow \pi^+ \nu \bar{\nu}$ [55], $K_L^0 \rightarrow \pi^0 \nu \bar{\nu}$ [56], the mass difference ΔM_K between K_L and K_S [43], and the indirect CP-violation ϵ_K in the $K - \bar{K}$ system [43]. When calculating these observables, we take into account theoretical uncertainties as well as those from CKM matrix, rare decays, and hadronic

parameters. The experimental limits of these constraints are as follows,

$$122.1 \text{ GeV} \leq m_h \leq 128.1 \text{ GeV}, \quad (34)$$

$$\Delta a_\mu = a_\mu^{\text{exp}} - a_\mu^{\text{SM}} = (24.9 \pm 8.7) \times 10^{-10}, \quad (35)$$

$$\Delta\rho < 8.8 \times 10^{-4}, \quad (36)$$

$$17.715 \text{ ps}^{-1} \leq \Delta M_s \leq 17.799 \text{ ps}^{-1}, \quad [2\sigma] \quad (37)$$

$$0.504 \text{ ps}^{-1} \leq \Delta M_d \leq 0.516 \text{ ps}^{-1}, \quad [2\sigma] \quad (38)$$

$$0.70 \times 10^{-4} \leq \text{BR}(B^\pm \rightarrow \tau^\pm \nu_\tau) \leq 1.58 \times 10^{-4}, \quad [2\sigma] \quad (39)$$

$$2.99 \times 10^{-4} \leq \text{BR}(\bar{B}^0 \rightarrow X_s \gamma) \leq 3.87 \times 10^{-4}, \quad [2\sigma] \quad (40)$$

$$1.7 \times 10^{-9} \leq \text{BR}(B_s^0 \rightarrow \mu^+ \mu^-) \leq 4.5 \times 10^{-9}, \quad [2\sigma] \quad (41)$$

$$0.84 \times 10^{-6} \leq \text{BR}(\bar{B}^0 \rightarrow X_s \ell^+ \ell^-)_{\text{low}} \leq 2.32 \times 10^{-6}, \quad [2\sigma] \quad (42)$$

$$2.8 \times 10^{-7} \leq \text{BR}(\bar{B}^0 \rightarrow X_s \ell^+ \ell^-)_{\text{high}} \leq 6.8 \times 10^{-7}, \quad [2\sigma] \quad (43)$$

$$2.7 \times 10^{-6} \leq \text{BR}(b \rightarrow d \gamma) \leq 25.5 \times 10^{-6}, \quad [2\sigma] \quad (44)$$

$$\text{BR}(B_d^0 \rightarrow \mu^+ \mu^-) \leq 8.7 \times 10^{-10}, \quad [3\sigma] \quad (45)$$

$$\text{BR}(B \rightarrow X_s \nu \bar{\nu}) < 6.4 \times 10^{-4}, \quad [90\% \text{CL}] \quad (46)$$

$$\text{BR}(B^+ \rightarrow K^+ \nu \bar{\nu}) < 1.6 \times 10^{-5}, \quad [90\% \text{CL}] \quad (47)$$

$$\text{BR}(B^0 \rightarrow K^{*0} \nu \bar{\nu}) < 5.5 \times 10^{-5}, \quad [90\% \text{CL}] \quad (48)$$

$$0.299 \leq R_D \leq 0.495, \quad [2\sigma] \quad (49)$$

$$0.259 \leq R_{D^*} \leq 0.373, \quad [3\sigma] \quad (50)$$

$$\text{BR}(K^+ \rightarrow \pi^+ \nu \bar{\nu}) < 4.03 \times 10^{-10}, \quad [2\sigma] \quad (51)$$

$$\text{BR}(K_L^0 \rightarrow \pi^0 \nu \bar{\nu}) < 2.6 \times 10^{-8}, \quad [90\% \text{CL}] \quad (52)$$

$$5.275 \times 10^{-3} \text{ ps}^{-1} \leq \Delta M_K \leq 5.311 \times 10^{-3} \text{ ps}^{-1}, \quad [2\sigma] \quad (53)$$

$$2.206 \times 10^{-3} \leq \epsilon_K \leq 2.250 \times 10^{-3}. \quad [2\sigma] \quad (54)$$

Various constraints from direct searches for new particles at colliders are relevant for the scenarios we consider. While scenarios with light sfermions are severely restricted by LEP, the LSP can be light enough to contribute to the Z_1 invisible decay width, we impose the constraint $\Delta\Gamma_{Z_1} < 0.5 \text{ MeV}$ [57].

Searches for a heavy neutral gauge boson in the dilepton and dijet channels have been performed at the LHC both at 8 TeV and 13 TeV. We use the most recent data on the dilepton final state corresponding to an integrated luminosity of 3.2 fb^{-1} at $\sqrt{s} = 13 \text{ TeV}$ [58]. Here, the Z_2 mass limit is interpolated for each specific value of θ_{E_6} . Limits from the dijet resonance searches at the LHC are obtained with the method described in Ref. [59] using a combination of

ATLAS [60,61] and CMS [62,63] dijet data at 8 TeV and 13 TeV. These constraints are included in micrOMEGAs4.3 [64]. In the UMSSM, there are cases where the lightest chargino is long-lived, typically when the chargino is nearly pure wino or nearly pure higgsino. For such points, we take into account the results from long-lived chargino searches at the Tevatron and the LHC. To derive this constraint, the observed limits for the cross sections of long-lived chargino pair production at D0 [65] experiment are employed in combination with the observed limit for chargino pair production and neutralino-chargino production cross section at the ATLAS [66] experiment. We follow the procedure described in [16].

In addition to the constraints from collider physics, we take into account those from cosmological observations. The most recent measurement of the DM relic density by Planck experiment [67] reads

$$\Omega_{\text{CDM}}h^2 = 0.1188 \pm 0.0010. \quad (55)$$

In the global parameter scan, we impose only an upper bound on the DM relic density of the LSP. Thus we implicitly assume that there could be an additional DM candidate.

For DM direct detection the LUX experiment sets the most severe constraint on the spin-independent (SI) cross section between a DM particle and nucleons [40, 68, 69], while PICO-60 [70] sets the best direct limit on the spin-dependent (SD) cross section on protons. The SD cross section on protons is also constrained by IceCube [71] by observing the neutrino flux from DM captured in the Sun, this limit however depends on specific annihilation channels.

The UMSSM model with kinetic mixing was implemented in LanHEP version 3.2.0 [72–74] which produces the model files suitable for CalcHEP [75]. The spectrum and all the DM observables are calculated using micrOMEGAs version 4.3.1 [15, 16, 64, 76] with the help of UMSSMTools [77] adapted from NMSSMTools v5.0.2 routines [78, 79]. The latter includes in particular all flavour physics observables. For collider observables, we use a routine of micrOMEGAs to compute the Z_2 limits from LHC as well as the Z_1 invisible width. An interface to HiggsBounds [80] allows to test the Higgs sector of the model with respect to 95% CL exclusion limits from the LEP, Tevatron and LHC experiments. Finally the points satisfying all the above collider constraints are analysed with SModelS 1.0.4 which decomposes the signal of any BSM model into simplified topologies in order to test it against LHC bounds [81, 82].

3.3 Benchmark analysis

We examine the effect of the kinetic mixing on the sparticle spectrum for a benchmark set of the UMSSM inputs. The simplified UMSSM input parameters are taken to be: the common gaugino masses $M'_1 = M_1 = M_2 = M_3 = M_G = 3$ TeV, the common slepton and squark soft

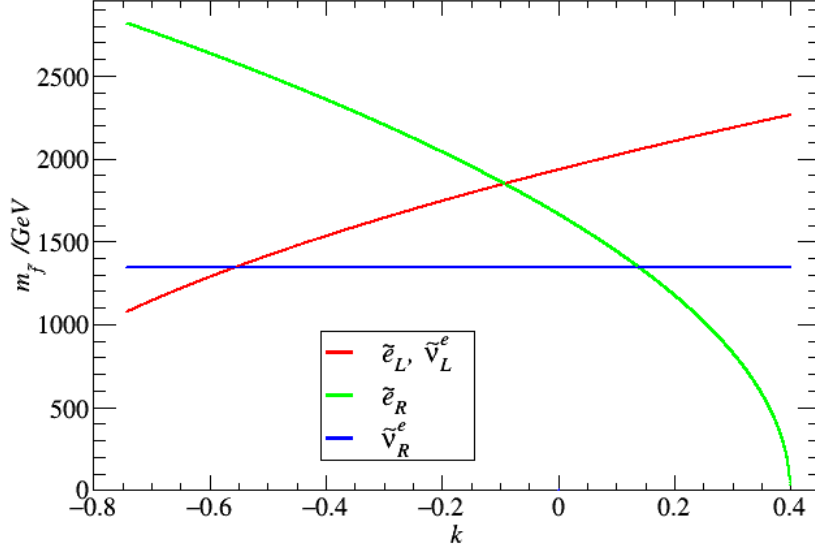


Figure 4: Slepton masses as functions of the gauge kinetic mixing k .

masses $m_{\tilde{l}}^0 = 1.1$ TeV and $m_{\tilde{q}}^0 = 3$ TeV respectively, the Z_2 boson mass $M_{Z_2} = 3.8$ TeV, the common trilinear coupling $A_0 = 3$ TeV, the μ -parameter $\mu = 1035.5$ GeV, the mixing angle between two Z -bosons $\alpha_Z = -0.64 \times 10^{-4}$, and the angle $\theta_{E_6} = 1.4$. Note that these values of μ, α_Z , and θ_{E_6} are chosen randomly such that all the phenomenological constraints, especially the 125 GeV Higgs boson mass and the DM relic abundance, can be satisfied for a suitable value of k . Letting the kinetic mixing parameter to be a free input, we find that the range with $-0.742 < k < 0.399$ is theoretically acceptable. The values outside this range are excluded by the reality condition (33) and the tachyonic slepton condition.

In Fig. 4, we show the dependence of slepton masses of the first generation on the kinetic mixing parameter. For this particular choice of inputs, the behaviors of the second and third slepton generations are very similar. The two sfermions belonging to the LH slepton doublet, $\tilde{\nu}_L^e$ and \tilde{e}_L , have masses too degenerate to be distinguished in the plot. When increasing the kinetic mixing, the LH slepton masses increase while the RH selectron mass decrease, becoming tachyonic for $k > 0.399$. The RH sneutrino mass is nearly independent on k .

Fig. 5 shows the first generation squark masses as functions the kinetic mixing parameter. Here, only the RH up-squark becomes heavier for larger k . The other squark masses (LH up-squark, LH down-squark, and RH down-squark) decrease with the kinetic mixing parameter k . As for the slepton case, the other two generations of squarks have a similar behavior as the first generation and are therefore not shown in the figure.

The k -dependence of sfermion masses can be explained using Eqs. (24), (16), and (18).

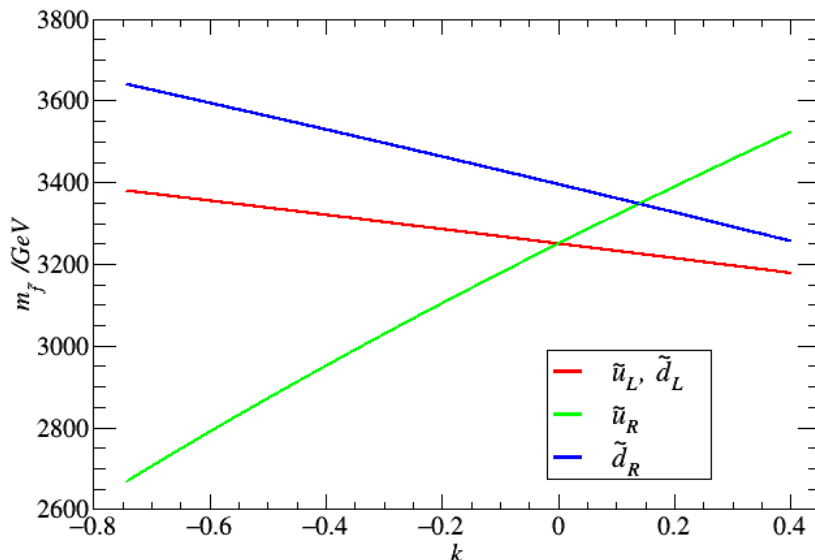


Figure 5: Squark masses as functions of the gauge kinetic mixing k .

Within the allowed range of k , corrections to the sfermion masses are dominantly controlled by $Q^p(k)$. For the benchmark value $\theta_{E_6} = 1.4$, the quantity in the brackets of the right side of (24) is positive. Therefore, the D-term correction to a sfermion mass is approximately proportional to $\frac{k}{1-k^2}$ and its hypercharge Y . The dependence on k is therefore stronger for the sparticle with a large hypercharge Y . The mass increases (decreases) with k for negative (positive) Y . The RH sneutrino has a hypercharge $Y_{\tilde{\nu}_R} = 0$, hence its mass remains almost constant. The kinetic mixing enters the neutralino masses only through the mixing between higgsinos, singlino and bino', hence the neutralino masses are almost independent of the kinetic mixing.

The SM-like Higgs boson mass is plotted as a function of the kinetic mixing k in Figs (6). We see that the Higgs boson mass decreases with k and that in the absence of kinetic mixing the mass would be much below the observed value. Thus, enabling a negative nonzero kinetic mixing, in this case $k \approx -0.7$, allows to bring the Higgs boson mass in agreement with the observed value, $m_h \sim 125$ GeV.

For illustration, we show in Tables 2, the sparticle mass spectrum as well as the constrained observables for the benchmark just discussed. Assuming theoretical uncertainties in the calculations, we find that only the muon g-2 and R_{D^*} satisfy the corresponding constraints at 3σ level, while all other observables comply with the experimental limits at 2σ level. The LEP limits, the invisible Z_1 width, and the dilepton and dijet constraints for the Z_2 boson from the LHC, the constraint from long-lived chargino searches at D0 and the ATLAS experiments are all satisfied. This benchmark is also compatible with limits on the Higgs sector obtained by

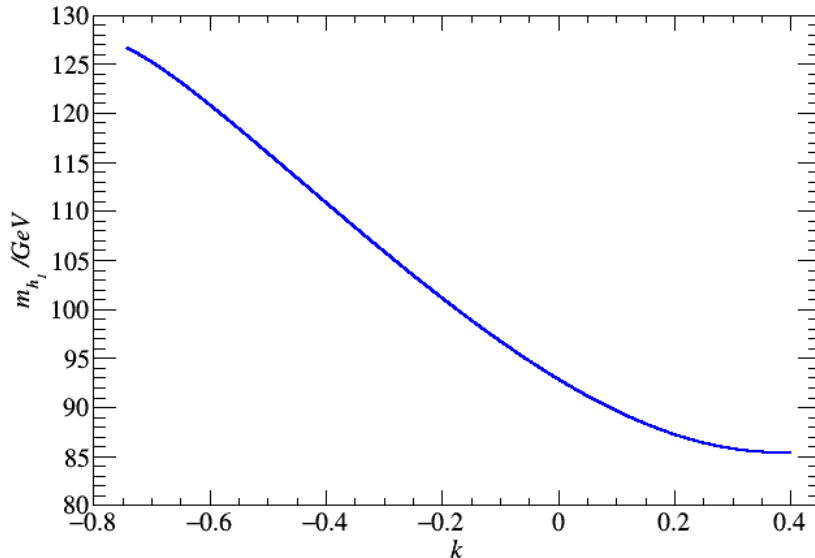


Figure 6: The SM-like Higgs boson mass as a function of the gauge kinetic mixing k .

Lilith and HiggsBounds as well as with limits on sparticles obtained with SModelS. We note that the kinetic mixing induces large shifts in the heavy Higgs doublet, from $\simeq 2.5$ TeV when $k = 0$ to $\simeq 5$ TeV when $k = -0.7$ while the singlet mass, m_{h_2} in Table 2, remains constant. Such heavy masses are in any case out of reach of the LHC. The DM candidate for this benchmark is a higgsino-like neutralino. Its relic density is achieved by annihilation into gauge bosons and coannihilation with the second lightest neutralino and the chargino NLSP whose masses are almost degenerate. The SI and SD cross sections of the DM scattering on nuclei meet the requirement from the LUX and IceCube experiments. Since the sparticles are quite heavy, it is challenging to test this benchmark at the LHC. However, the future XENON1T will be able to test the model via the SI interaction of the neutralino DM.

3.4 Global parameter scan

We assume that squark and slepton soft masses of the first two generations are universal, $m_{\tilde{f}_1} = m_{\tilde{f}_2}$ where $f = \{q, u, d, l, \nu, e\}$, and the trilinear couplings of the first two generations are negligible. We are thus left with 25 free parameters including the gauge kinetic mixing. The

Inputs		Mass spectrum		Observables	
M_G	3000	h_1	125.2	Δa_μ	3.182×10^{-11}
$m_{\tilde{l}}^0$	1100	h_2	3800	$\Delta \rho$	1.616×10^{-6}
$m_{\tilde{q}}^0$	3000	h_3	5024	ΔM_s	16.83 ps^{-1}
M_{Z_2}	3800	A^0	5024	ΔM_d	0.485 ps^{-1}
A_0	3000	H^\pm	5025	$\text{BR}(B^\pm \rightarrow \tau^\pm + \nu_\tau)$	1.070×10^{-4}
μ	1035.5	Z_2	3800	$\text{BR}(\bar{B}^0 \rightarrow X_s \gamma)$	3.347×10^{-4}
α_Z	-0.64×10^{-4}	\tilde{g}	3000	$\text{BR}(\bar{B}_s^0 \rightarrow \mu^+ \mu^-)$	3.346×10^{-9}
θ_{E_6}	1.4	$\tilde{\chi}_{1,2}^0$	1033, 1036	$\text{BR}(\bar{B}^0 \rightarrow X_s \ell^+ \ell^-)_{\text{low}}$	1.671×10^{-6}
k	-0.7	$\tilde{\chi}_{3,4}^0$	2586, 3000	$\text{BR}(\bar{B}^0 \rightarrow X_s \ell^+ \ell^-)_{\text{high}}$	2.401×10^{-7}
		$\tilde{\chi}_{5,6}^0$	3003, 5586	$\text{BR}(b \rightarrow d \gamma)$	1.73×10^{-5}
		$\tilde{\chi}_{1,2}^\pm$	1034, 3003	$\text{BR}(B_d^0 \rightarrow \mu^+ \mu^-)$	9.62×10^{-11}
		$\tilde{\nu}_{L,R}^{e,\mu}$	1141, 1345	$\text{BR}(B \rightarrow X_s \nu \bar{\nu})$	2.89×10^{-5}
		$\tilde{e}, \tilde{\mu}_{L,R}$	1144, 2764	$\text{BR}(B^+ \rightarrow K^+ \nu \bar{\nu})$	3.96×10^{-6}
		$\tilde{\nu}_{L,R}^\tau$	1141, 1100	$\text{BR}(B^0 \rightarrow K^{*0} \nu \bar{\nu})$	9.15×10^{-6}
		$\tilde{\tau}_{1,2}$	1144, 2764	R_D	0.297
		$\tilde{u}, \tilde{c}_{L,R}$	3372, 2705	R_{D^*}	0.252
		$\tilde{d}, \tilde{s}_{L,R}$	3373, 3626	$\text{BR}(K^+ \rightarrow \pi^+ \nu \bar{\nu})$	8.60×10^{-11}
		$\tilde{t}_{1,2}$	2700, 3385	$\text{BR}(K_L^0 \rightarrow \pi^0 \nu \bar{\nu})$	2.70×10^{-11}
		$\tilde{b}_{1,2}$	3374, 3626	ΔM_K	5.80×10^{-3}
				ϵ_K	1.86×10^{-3}
				Ωh^2	0.1188
				$\sigma_{SI}^{\chi^- p}$	2.727×10^{-10}
				$\sigma_{SD}^{\chi^- p}$	1.840×10^{-7}

Table 2: The sparticle mass spectrum in GeV and the corresponding constrained observables for the given set of input parameters.

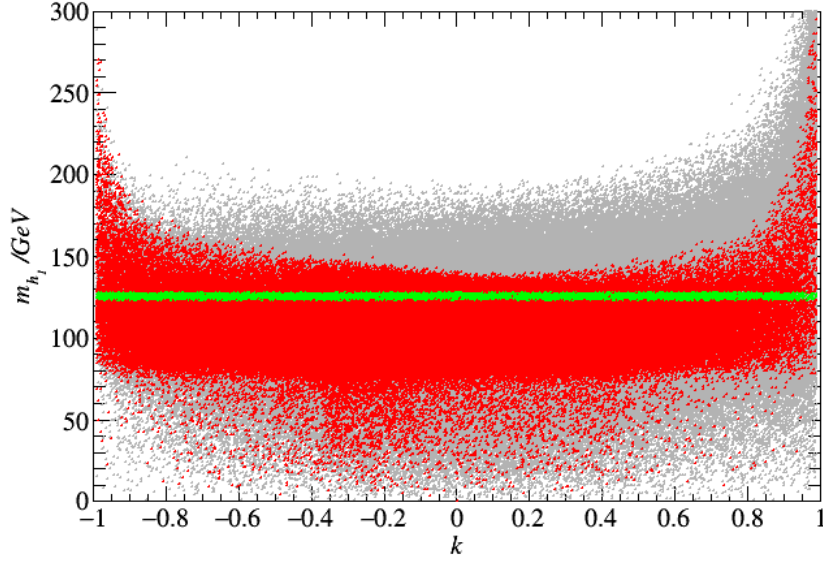


Figure 7: Theoretically allowed points in the plane (k, m_{h_1}) . Grey points are excluded by flavour constraints, LEP mass limits, invisible Z_1 decay width, LHC searches for a Z_2 boson, and searches for long-lived chargino, red points are excluded by Higgs mass constraints as well as HiggsBounds and Lilith. Green points satisfy all constraints.

ranges for these parameters are chosen as follows

$$-2000 < M_1, M_2, \mu < 2000 \text{ (GeV)} \quad (56)$$

$$100 < M_3 < 4000 \text{ (GeV)}, \quad (57)$$

$$10 < M'_1 < 4000 \text{ (GeV)}, \quad (58)$$

$$0 < m_{\tilde{q}_i}, m_{\tilde{u}_i}, m_{\tilde{d}_i} < 4000 \text{ (GeV)}, \quad i = \{1, 2, 3\} \quad (59)$$

$$0 < m_{\tilde{l}_i}, m_{\tilde{\nu}_j}, m_{\tilde{\nu}_{\tau R}}, m_{\tilde{e}_i} < 2000 \text{ (GeV)}, \quad i = \{1, 2, 3\}, j = \{1, 2\} \quad (60)$$

$$-4000 < A_\lambda, A_t, A_b, A_\tau < 4000 \text{ (GeV)}, \quad (61)$$

$$-10^{-3} < \alpha_Z < 10^{-3}, \quad (62)$$

$$1000 < M_{Z_2} < 8000 \text{ (GeV)}, \quad (63)$$

$$-\frac{\pi}{2} < \theta_{E_6} < \frac{\pi}{2}, \quad (64)$$

$$-1 < k < 1. \quad (65)$$

We have performed a random scan over this parameter region with 5×10^8 points. The particle mass spectrum and all the above constrained observables have been calculated for each point. Only points satisfying the theoretical constraints are considered in our analysis.

In Fig. 7, a scatter plot is shown in the plane (k, m_{h_1}) . Looking at the density in the plot, most of the points correspond to a Higgs mass between 50 GeV and 180 GeV. Clearly

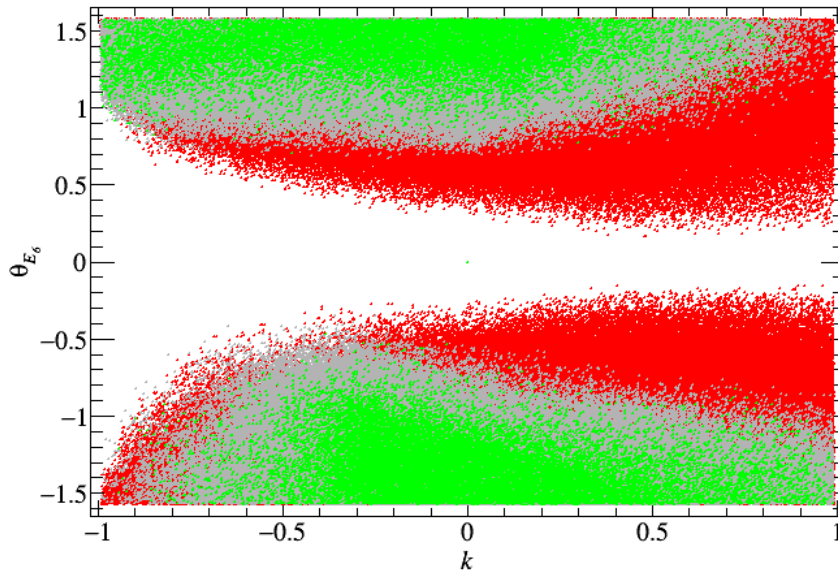


Figure 8: Allowed region in the plane k, θ_{E_6} (in green). Red points are excluded by Z_2 searches while grey points are excluded by all other constraints.

the Higgs mass in this model can be enhanced with the nonzero gauge kinetic mixing and the effect of nonzero kinetic mixing can be quite large for $|k| \in (0.8, 1.0)$. This is due to the $U(1)'$ D-term contribution (the third term in Eq. (29)) proportional to the gauge coupling g_E that is greatly enhanced for large k . Nevertheless, the value $m_{h_1} \simeq 125$ GeV can be obtained for any value of the kinetic mixing. Note that the constraints from flavour physics (36)-(54) and $(g-2)_\mu$ (35) are most severe in the low Higgs mass region $m_{h_1} \lesssim 80$ GeV and relatively small kinetic mixing, a region that is in any case not physically interesting. For $m_{h_1} \simeq 125$ GeV, the constraint from Z_2 searches plays a very important role while the searches for long-lived chargino do not provide a significant constraint after all other phenomenological constraints are taken into account. The impact of the Z_2 searches and other collider constraints is best illustrated in the plane (k, θ_{E_6}) , see Fig. 8. The Z_2 constraint is particularly important in the region with large kinetic mixing $k \gtrsim 0.5$ due to the enhancement of the coupling g_E , it has also an impact for large negative values of the kinetic mixing although for these values theoretical constraints are more important and only allow a restricted range for θ_{E_6} .

It is interesting to observe that because of the non zero kinetic mixing, the LHC constraints on the Z_2 mass can be significantly relaxed. Typically the current limit is around 2.8 TeV with a slight dependence on θ_{E_6} . However for certain values of θ_{E_6} and k the coupling of the Z_2 to the RH leptons is strongly suppressed due to a cancellation between the two terms in Eq. 18. Hence without an increase in the coupling to LH leptons or quarks to compensate, the limit

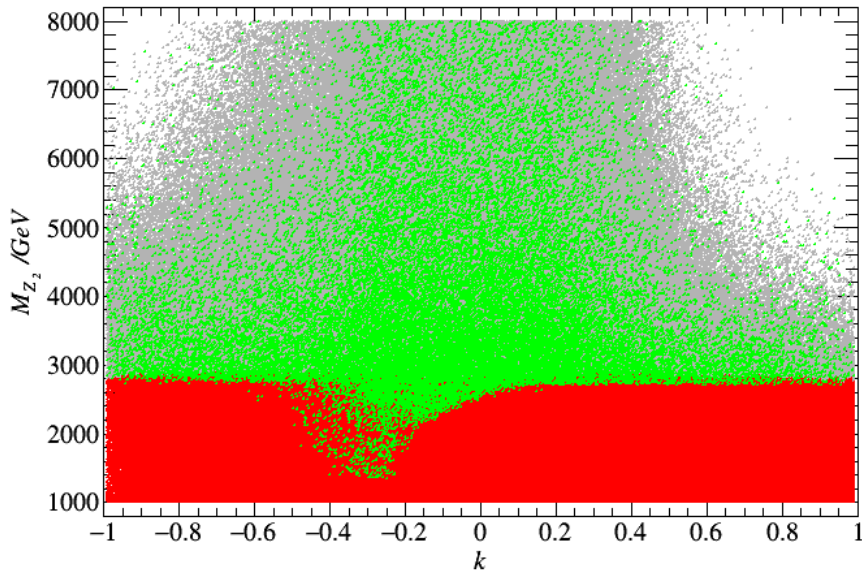


Figure 9: Allowed region in the plane k, M_{Z_2} (in green). The color code is the same as in Fig. 8.

on the Z_2 boson mass from dileptons is relaxed and can drop below 2 TeV. This occurs for $-1.2 < \theta_{E_6} < -0.8$ and $-0.45 < k < -0.15$, see Fig. 9. The lightest allowed value is found to be $M_{Z_2} = 1.3$ TeV.

The predictions for the muon anomalous magnetic moment are presented in Fig. 10. It is possible, for any value of k to reproduce the central value for for this observable, Eq. 35. In particular Δa_μ can be enhanced by a relatively light Z_2 , this is because a small M_{Z_2} implies a small Higgs singlet VEV, v_S , (see Eq. (20)) which in turn can result in a small $U(1)'$ D-term corrections to smuon masses (Eq. 24). However after taking into account the LHC constraints on the Z_2 boson, the number of points with $\Delta a_\mu \approx 10^{-9}$ is significantly reduced especially at large k . In addition the region of parameter space where the Z_2 mass can be relaxed does not correspond to the one leading to a large contribution to Δa_μ . Other constraints also restrict the allowed regions. In the flavour sector (also shown in grey in Fig. 10), the constraints on ΔM_s (37) and ΔM_d (38) are quite important but mostly for the region with low $\Delta a_\mu < 10^{-11}$. while for $\Delta a_\mu \gtrsim 10^{-10}$, the constraints from $\bar{B}^0 \rightarrow X_s \gamma$ (40) are more severe. Note that the constraints for the branching ratio of $B_d^0 \rightarrow \mu^+ \mu^-$ and R_{D^*} are particularly severe and that we have used the 3σ bounds for them. As mentioned above, the constraints on the Higgs sector (in red) have a strong impact on the parameter space, they rule out a large number of points with low Δa_μ , but also some points at large k where the prediction for Δa_μ is within the 2σ observed range. It is worth noting that within our scan, there are no green points with $\Delta a_\mu \gtrsim 2 \times 10^{-9}$

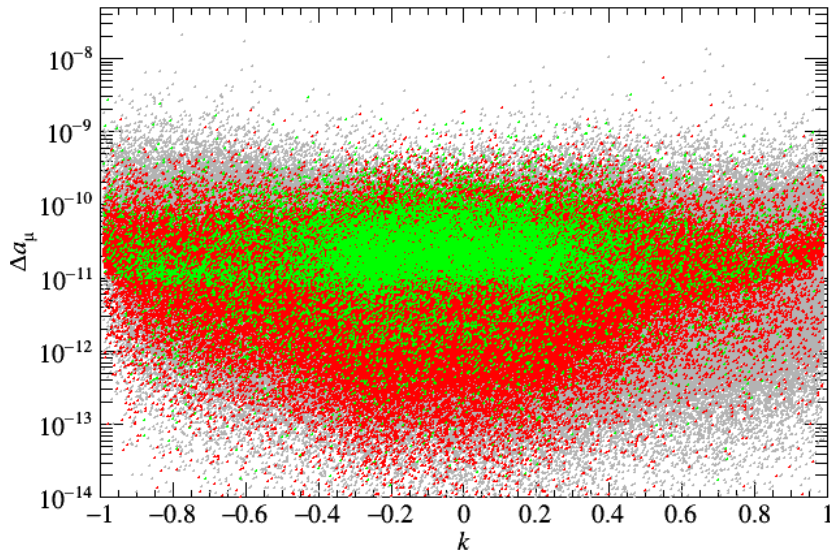


Figure 10: The anomalous magnetic moment of the muon, Δa_μ vs the gauge kinetic mixing k . Green points are allowed, red points are excluded by constraints on the Higgs mass and couplings and grey points are excluded by all other flavour and collider constraints. The green points are plotted on top of the other ones.

in the region $|k| < 0.2$, while we can find such green points for the regions $|k| > 0.2$. Therefore, even after taking into account all constraints, there is some enhancement in the predicted value of the muon $g - 2$ although it is small.

We now discuss dark matter observables including the relic density and DM elastic scattering cross section on nuclei. In the numerical results we consider only points that successfully predict a Higgs boson mass in the range $[122, 128]$ GeV and that satisfy collider and flavour constraints. Points with a charged/colored LSP are not considered as they are disfavored by cosmological observations. There are two possibilities for DM in this model, the lightest neutralino or the RH sneutrino, recall that the LH sneutrino LSP typically leads to a large SI cross section on nuclei due to the exchange of a Z_1 boson and are thus excluded by DM direct detection experiments [26]. We do not consider this possibility. Fig. 11 shows the scatter plot of the collider allowed points in the plane (k, m_{LSP}) , including both the neutralino-LSP (green) as well as the RH sneutrino-LSP (red). The latter is much less likely. Moreover we observe that in the region with small $|k|$ there are more possibilities to have a heavy DM than in the region with large $|k|$. In particular most of the points associated with a DM candidate with a mass $m_{\text{LSP}} \geq 1200$ GeV have relatively small kinetic mixing $|k| \leq 0.5$. This is related to the fact that large kinetic mixing induces a shift in some of the sfermion masses and are therefore more likely to have a charged LSP and moreover that more points are excluded by the LHC search

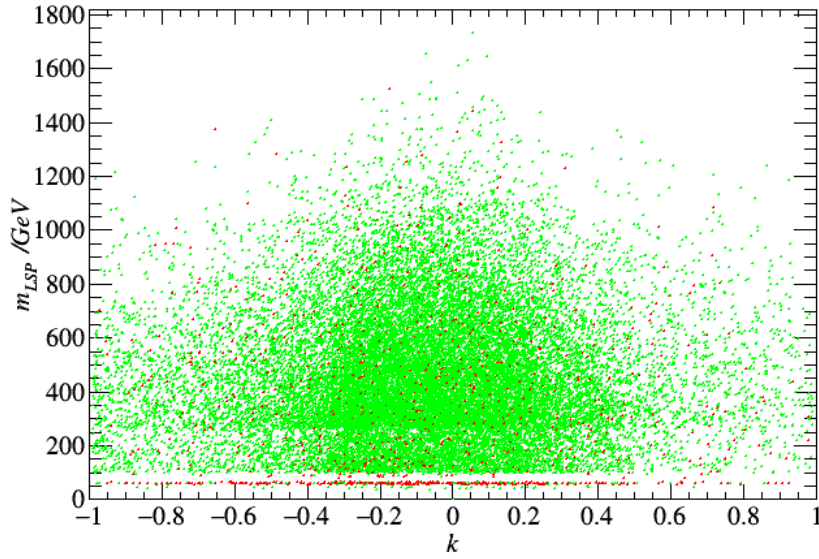


Figure 11: The scatter plot on the plane (k, m_{LSP}) for the neutralino-LSP (green) and the RH sneutrino-LSP (red). All the points satisfy the collider and flavour constraints as well as the upper bound on the relic density.

for Z_2 boson due to its enhanced coupling for large $|k|$, see Fig. 8. Note that Fig. 11 shows only the points that satisfy the relic density upper bound from PLANCK, however the distribution of points is similar without the constraint except for the region with a very light LSP.

The DM relic density for each type of DM is presented in the scatter plot of Fig. 12. We find as expected that the RH sneutrino DM is typically overabundant since it is very weakly coupled to SM particles. There are however special cases where the RH sneutrino predicts a relic density in agreement or below the PLANCK value. When the RH sneutrino mass is near $m_{h_1}/2$, the DM annihilation is enhanced by a resonance effect, similarly when the mass is near $m_{Z_2}/2$. Considering the LHC constraint on the Z_2 , this requires a rather heavy sneutrino DM. Finally there is always the possibility of coannihilation with other sfermions or neutralino/chargedino. The latter can occur for any mass. Although there is an impact of the gauge kinetic mixing in these scenarios since the masses of the Higgs, Z_2 and sfermions all depend on the kinetic mixing, in the global scan there is no direct correlation between the relic density and the kinetic mixing, and a value $\Omega h^2 \sim 0.1$ can be obtained for the whole range of k . This statement also holds for neutralino DM.

The value of the relic density for neutralino DM (in green in Fig. 12) features a strong dependence on the nature of the LSP. Most of the points with overabundant DM are associated with a bino or singlino LSP while those with underabundant DM correspond to higgsino-like and wino-like LSP. These are clustered in the two strips at the bottom of Fig. 12 that extend

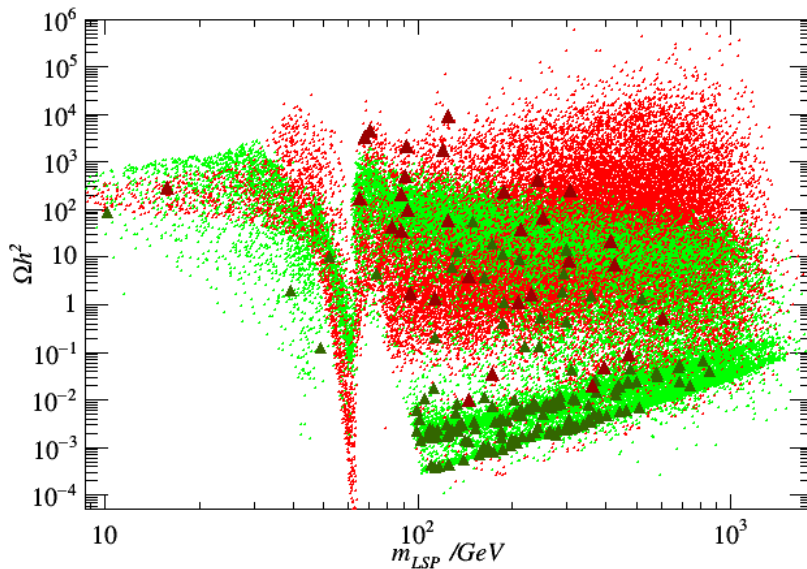


Figure 12: The scatter plot on the plane $(m_{\text{LSP}}, \Omega h^2)$. The color codes are the same as in Fig. 11. Triangles: points satisfying the muon $g - 2$ limits at 2σ level and SModelS test in addition to other collider constraints.

from 100 GeV to 2 TeV, the wino-like LSP corresponding to the points with the lower value of the relic density. Note that we find only a few points with \tilde{S} -like LSP, and no point with \tilde{B}' -like LSP. Other green points predicting the allowed DM relic density are either well-tempered neutralino or bino-like neutralinos with co-annihilation. They scatter in a large mass range. For $m_{\text{LSP}} \lesssim 100$ GeV, and $\Omega h^2 \lesssim 0.1$, we find that the only possibility for the neutralino LSP to have an acceptable relic density is the Higgs-resonance region where the DM mass is about half the SM-like Higgs or Z_1 boson mass, $m_{\text{LSP}} \sim 62$ GeV or $m_{\text{LSP}} \sim 45$ GeV. Here, neutralino annihilation mainly happens via the Higgs (Z_1) exchange in the s-channel. Altogether most of the points which satisfy the relic density upper bound are associated with a compressed spectra, in particular with a NLSP nearly degenerate with the LSP. Indeed such spectra is found for dominantly higgsino and wino neutralino as well as for coannihilation of neutralino or sneutrino. Because of the strong constraints from LEP on light charged particles below 100 GeV, coannihilation in this region is not possible. In addition several points (especially for sneutrino DM) are clustered around $m_{h_1}/2$, only a few points feature uncorrelated a large mass splitting between the NLSP and the LSP.

The SD cross section for DM scattering on nuclei relevant to direct DM searches and to indirect searches with neutrino telescopes is shown in Fig. (13) for all the points satisfying the collider constraints and the upper limit of DM relic density from Planck ($\Omega h^2 < 0.1208$). Note that this figure includes only the neutralino-LSP since the sneutrino-LSP is a scalar particle

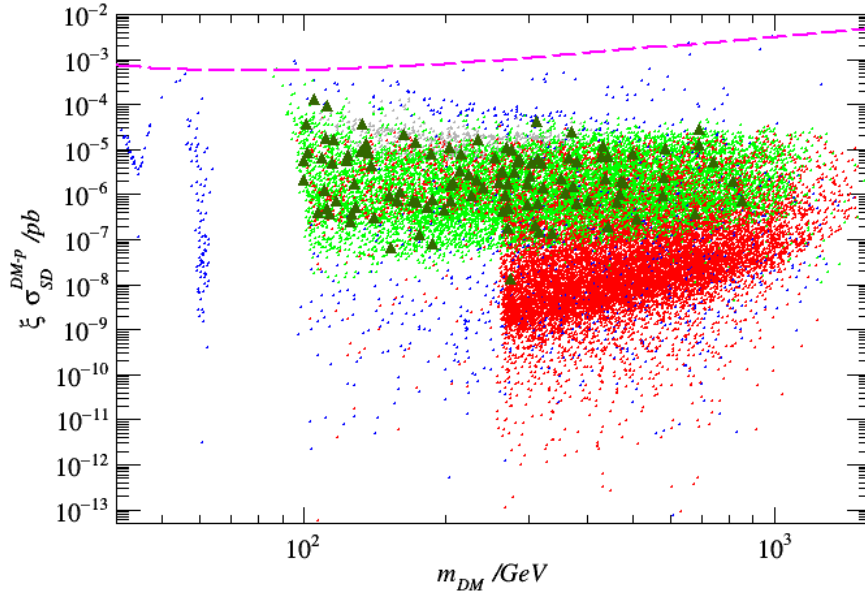


Figure 13: The scatter plot on the plane $(m_{DM}, \xi \sigma_{SD}^{\text{DM-p}})$. Grey points are excluded by the IceCube constraint. Other colored points satisfy all collider constraints, as well as the upper limit of DM relic density from Planck and the upper limit of SD cross section from IceCube. Blue: bino-like LSP, red: wino-like LSP, green: higgsino-like LSP. Triangles are a subset of green points, and satisfy the muon $g - 2$ limits at 2σ level as well as SModelS test. Dashed pink curve: PICO upper limit.

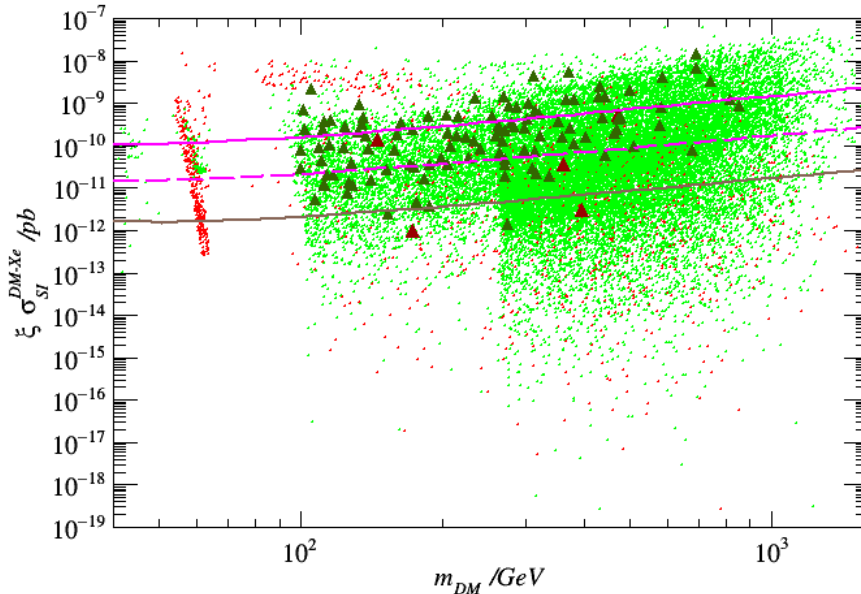


Figure 14: The scatter plot on the plane $(m_{DM}, \sigma_{SI}^{DM-Xe})$. All the points satisfy the collider constraints, as well as the upper limit of DM relic density from Planck and the upper limit of SD cross section from IceCube. The color codes are the same as in Fig. 11. Among these points, the triangles represent points satisfying the muon $g - 2$ limits at 2σ level as well as SModelS test. The pink, dashed pink, and brown curves indicate the upper limit set by LUX experiment [40], the projected XENON1T and XENONnT [83] respectively.

and does not have SD interaction with nuclei. To take into account the fact that neutralino DM may account only for a fraction of the DM content of the universe, we rescale the cross section for cases where DM is underabundant by $\xi = \Omega h^2 / 0.1188$. In the figure, points satisfying the muon $g - 2$ at 2σ level and all other collider constraints including LHC limits from SModelS are marked by triangles. Moreover, we impose the IceCube limit as described in Ref [84], the points ruled out by this constraint are shown as grey dots. The direct detection limit from PICO [70] is also displayed as a pink dashed line, this limit is easily satisfied for most of the points since they lie generally two orders of magnitude below the current limit. The sharp cut in the plot around 250 GeV is due to the constraint from searches for long-lived chargino.

Fig. 14 shows the rescaled SI cross section with respect to the DM mass. The color codes are the same as in Fig. 11. When the LSP is the RH sneutrino, a significant fraction of the scenarios are clustered around $m_{LSP} \approx m_{h_1} / 2$ in order to benefit from resonance annihilation in the early universe. The points that are further away from the resonance and that require a larger coupling to the Higgs lead to a large direct detection cross section and are excluded by LUX. Other points where the coupling to the Higgs is small predict a SI cross section that can be below the expected limit from XENONnT. Other scenarios with a RH sneutrino are ruled

out by the LUX constraint, typically those that have a large coupling to the Higgs while others that rely on co-annihilation predict a cross section orders of magnitude below the sensitivity of ton-scale experiments. The LUX limit excludes a considerable number of points with the neutralino-LSP (green dots). Especially, the LUX limit rules out several of the points that are compatible with muon $g - 2$ at 2σ level (triangles). In fact, with the expected sensitivity of the ton-scale experiments (for example the projected sensitivity of XENON1T as represented by the pink dashed curve), if no DM signal is observed it will introduce a severe tension for the model to reconcile both the muon anomalous magnetic moment and the SI cross section between the neutralino-LSP and nuclei while satisfying all other constraints. However, if we relax the muon $g - 2$ constraint to 3σ bounds, there are several neutralino-LSP scenarios, as in the MSSM, which can escape the most sensitive future direct detection experiments such as XENONnT [83], typically they are associated with wino or higgsino LSP.

4 Conclusions

We have implemented the gauge kinetic mixing in the UMSSM and have found that the kinetic mixing has an important effect on the mass spectrum and on the coupling of the Z_2 boson with fermions. Especially, the mass of the SM-like Higgs boson can be significantly enhanced by an appropriate choice of the kinetic mixing. This then impacts physical observables and has been illustrated for a benchmark point. After applying various theoretical and phenomenological constraints and performing a global parameter scan we have shown that for specific values of the kinetic mixing it is possible to relax the current constraint on the Z_2 boson mass ($M_{Z_2} \lesssim 2.8$ TeV) to as low as 1.3 TeV when its dilepton branching ratio is suppressed. We have also found that the predictions for Δa_μ in scenarios with gauge kinetic mixing can in some cases be within 2σ of the measured value, thus releasing some of the tension on this observable. The properties of the LSP and the DM relic density have been examined, and it is found that agreement with the observed value of the relic density could be obtained for any value of the kinetic mixing. Both neutralino and RH sneutrino can be viable DM candidates. Moreover direct DM searches play an important role in ruling out large portions of the parameter space and offer good prospects of probing the model further although not completely. This is a feature shared with the MSSM. The RH sneutrino in particular can lead to very small scattering cross sections on nuclei.

The upcoming LHC runs with improved reach for the search of a Z_2 boson will provide further decisive tests of the model, both in the dilepton and dijet modes. The latter being crucial to probe the cases where the branching ratios of Z_2 into dileptons is suppressed because of the kinetic mixing. SUSY searches are more challenging since the model often features a

compressed spectra, although searches for long-lived charged particles will probe a fraction of the compressed scenarios.

Acknowledgment

The authors are grateful to Alexander Pukhov and Ursula Laa for useful discussions. H.M.T. would like to thank LAPTh, especially Patrick Aurenche, for hospitality and support during his visit. This work is supported by the “Investissements d’avenir, Labex ENIGMASS” and by the French ANR, Project DMAstro-LHC, ANR-12-BS05-006. The work of H.M.T. is partly supported by Vietnam National Foundation for Science and Technology Development (NAFOSTED) under the grant No. 103.01-2014.22.

References

- [1] G. Aad *et al.* [ATLAS Collaboration], Phys. Lett. B **716**, 1 (2012) [arXiv:1207.7214 [hep-ex]].
- [2] S. Chatrchyan *et al.* [CMS Collaboration], Phys. Lett. B **716**, 30 (2012) [arXiv:1207.7235 [hep-ex]].
- [3] L. J. Hall, D. Pinner and J. T. Ruderman, JHEP **1204**, 131 (2012) [arXiv:1112.2703 [hep-ph]].
- [4] J. E. Camargo-Molina, B. O’Leary, W. Porod and F. Staub, JHEP **1312**, 103 (2013) [arXiv:1309.7212 [hep-ph]].
- [5] N. Blinov and D. E. Morrissey, JHEP **1403**, 106 (2014) [arXiv:1310.4174 [hep-ph]].
- [6] D. Chowdhury, R. M. Godbole, K. A. Mohan and S. K. Vempati, JHEP **1402**, 110 (2014) [arXiv:1310.1932 [hep-ph]].
- [7] J. Cao, Z. Heng, D. Li and J. M. Yang, Phys. Lett. B **710**, 665 (2012) [arXiv:1112.4391 [hep-ph]].
- [8] N. Okada and H. M. Tran, Phys. Rev. D **87**, no.3, 035024 (2013) [arXiv:1212.1866 [hep-ph]].
- [9] N. Okada and H. M. Tran, Phys. Rev. D **94**, no. 7, 075016 (2016) [arXiv:1606.05329 [hep-ph]].

- [10] W. Yin and N. Yokozaki, Phys. Lett. B **762**, 72 (2016) [arXiv:1607.05705 [hep-ph]].
- [11] A. Aboubrahim, T. Ibrahim and P. Nath, Phys. Rev. D **94**, no. 1, 015032 (2016) [arXiv:1606.08336 [hep-ph]].
- [12] V. Barger, P. Langacker, M. McCaskey, M. Ramsey-Musolf and G. Shaughnessy, Phys. Rev. D **79**, 015018 (2009) [arXiv:0811.0393 [hep-ph]].
- [13] P. Athron, S. F. King, D. J. Miller, S. Moretti and R. Nevzorov, Phys. Rev. D **80**, 035009 (2009) [arXiv:0904.2169 [hep-ph]]; P. Athron, S. F. King, D. J. Miller, S. Moretti and R. Nevzorov, Phys. Rev. D **86**, 095003 (2012) [arXiv:1206.5028 [hep-ph]]; P. Athron, D. Stockinger and A. Voigt, Phys. Rev. D **86**, 095012 (2012) [arXiv:1209.1470 [hep-ph]]; P. Athron, D. Harries and A. G. Williams, Phys. Rev. D **91**, 115024 (2015) [arXiv:1503.08929 [hep-ph]].
- [14] M. Hirsch, W. Porod, L. Reichert and F. Staub, Phys. Rev. D **86**, 093018 (2012) [arXiv:1206.3516 [hep-ph]].
- [15] G. Belanger, J. Da Silva and A. Pukhov, JCAP **1112**, 014 (2011) [arXiv:1110.2414 [hep-ph]].
- [16] G. Bélanger, J. Da Silva, U. Laa and A. Pukhov, JHEP **1509**, 151 (2015) [arXiv:1505.06243 [hep-ph]].
- [17] U. Ellwanger and C. Hugonie, JHEP **1408**, 046 (2014) [arXiv:1405.6647 [hep-ph]].
- [18] A. Kaminska, G. G. Ross, K. Schmidt-Hoberg and F. Staub, JHEP **1406**, 153 (2014) [arXiv:1401.1816 [hep-ph]].
- [19] M. Farina, M. Perelstein and B. Shakya, JHEP **1404**, 108 (2014) [arXiv:1310.0459 [hep-ph]].
- [20] P. Athron, M. Binjonaid and S. F. King, Phys. Rev. D **87**, no.11, 115023 (2013) [arXiv:1302.5291 [hep-ph]].
- [21] M. Cvetič, D. A. Demir, J. R. Espinosa, L. L. Everett and P. Langacker, Phys. Rev. D **56**, 2861 (1997) Erratum: [Phys. Rev. D **58**, 119905 (1998)] [hep-ph/9703317].
- [22] V. Barger, P. Langacker, H. S. Lee and G. Shaughnessy, Phys. Rev. D **73**, 115010 (2006) [hep-ph/0603247].
- [23] P. Langacker and J. Wang, Phys. Rev. D **58**, 115010 (1998) [hep-ph/9804428].

- [24] M. Cvetič and P. Langacker, *Phys. Rev. D* **54**, 3570 (1996) [hep-ph/9511378].
- [25] M. Cvetič and P. Langacker, *Mod. Phys. Lett. A* **11**, 1247 (1996) [hep-ph/9602424].
- [26] T. Falk, K. A. Olive and M. Srednicki, *Phys. Lett. B* **339**, 248 (1994) doi:10.1016/0370-2693(94)90639-4 [hep-ph/9409270].
- [27] B. Holdom, *Phys. Lett. B* **166**, 196 (1986).
- [28] P. H. Chankowski, S. Pokorski and J. Wagner, *Eur. Phys. J. C* **47**, 187 (2006) [hep-ph/0601097].
- [29] B. Brahmachari and A. Raychaudhuri, *Nucl. Phys. B* **887**, 441 (2014) [arXiv:1409.2082 [hep-ph]].
- [30] K. S. Babu, C. F. Kolda and J. March-Russell, *Phys. Rev. D* **57**, 6788 (1998) [hep-ph/9710441].
- [31] F. del Aguila, G. D. Coughlan and M. Quiros, *Nucl. Phys. B* **307**, 633 (1988) Erratum: [Nucl. Phys. B **312** (1989) 751].
- [32] F. del Aguila, J. A. Gonzalez and M. Quiros, *Nucl. Phys. B* **307**, 571 (1988).
- [33] R. M. Fonseca, M. Malinsky, W. Porod and F. Staub, *Nucl. Phys. B* **854**, 28 (2012) [arXiv:1107.2670 [hep-ph]].
- [34] B. O’Leary, W. Porod and F. Staub, *JHEP* **1205**, 042 (2012) [arXiv:1112.4600 [hep-ph]].
- [35] K. S. Babu, C. F. Kolda and J. March-Russell, *Phys. Rev. D* **54**, 4635 (1996) [hep-ph/9603212]; G. C. Cho, K. Hagiwara and Y. Umeda, *Nucl. Phys. B* **531**, 65 (1998) Erratum: [Nucl. Phys. B **555**, 651 (1999)] Erratum: [Nucl. Phys. B **565**, 483 (2000)] [hep-ph/9805448]; G. C. Cho, N. Maru and K. Yotsutani, *Mod. Phys. Lett. A* **31**, no. 22, 1650130 (2016) [arXiv:1602.04271 [hep-ph]].
- [36] L. Basso, B. O’Leary, W. Porod and F. Staub, *JHEP* **1209**, 054 (2012) [arXiv:1207.0507 [hep-ph]].
- [37] J. Kalinowski, S. F. King and J. P. Roberts, *JHEP* **0901**, 066 (2009) doi:10.1088/1126-6708/2009/01/066 [arXiv:0811.2204 [hep-ph]].
- [38] P. Athron, A. W. Thomas, S. J. Underwood and M. J. White, *Phys. Rev. D* **95**, no. 3, 035023 (2017) [arXiv:1611.05966 [hep-ph]].

- [39] P. Athron, D. Harries, R. Nevzorov and A. G. Williams, Phys. Lett. B **760**, 19 (2016) [arXiv:1512.07040 [hep-ph]]; P. Athron, D. Harries, R. Nevzorov and A. G. Williams, JHEP **1612**, 128 (2016) [arXiv:1610.03374 [hep-ph]].
- [40] D. S. Akerib *et al.* [LUX Collaboration], Phys. Rev. Lett. **118**, no. 2, 021303 (2017) [arXiv:1608.07648 [astro-ph.CO]].
- [41] S. F. King, S. Moretti and R. Nevzorov, Phys. Rev. D **73**, 035009 (2006) [hep-ph/0510419].
- [42] G. Aad *et al.* [ATLAS and CMS Collaborations], Phys. Rev. Lett. **114**, 191803 (2015) [arXiv:1503.07589 [hep-ex]].
- [43] K. A. Olive *et al.* [Particle Data Group Collaboration], Chin. Phys. C **38**, 090001 (2014).
- [44] G. W. Bennett *et al.* [Muon g-2 Collaboration], Phys. Rev. D **73**, 072003 (2006) [hep-ex/0602035].
- [45] B. L. Roberts, Chin. Phys. C **34**, 741 (2010) [arXiv:1001.2898 [hep-ex]].
- [46] T. Aoyama, M. Hayakawa, T. Kinoshita and M. Nio, Phys. Rev. Lett. **109**, 111808 (2012) [arXiv:1205.5370 [hep-ph]].
- [47] Y. Amhis *et al.* [Heavy Flavor Averaging Group (HFAG) Collaboration], arXiv:1412.7515 [hep-ex].
- [48] Heavy Flavor Averaging Group. <http://www.slac.stanford.edu/xorg/hfag/rare/2013/rad11/OUTPUT>
- [49] Heavy Flavor Averaging Group. <http://www.slac.stanford.edu/xorg/hfag/rare/2013/rad11/btos>
- [50] T. Huber, T. Hurth and E. Lunghi, JHEP **1506**, 176 (2015) [arXiv:1503.04849 [hep-ph]].
- [51] P. del Amo Sanchez *et al.* [BaBar Collaboration], Phys. Rev. D **82**, 051101 (2010) [arXiv:1005.4087 [hep-ex]].
- [52] A. Crivellin and L. Mercolli, Phys. Rev. D **84**, 114005 (2011) [arXiv:1106.5499 [hep-ph]].
- [53] R. Barate *et al.* [ALEPH Collaboration], Eur. Phys. J. C **19**, 213 (2001) [hep-ex/0010022].
- [54] Heavy Flavor Averaging Group. <http://www.slac.stanford.edu/xorg/hfag/semi/winter16/winter>
- [55] A. V. Artamonov *et al.* [E949 Collaboration], Phys. Rev. Lett. **101**, 191802 (2008) [arXiv:0808.2459 [hep-ex]].

- [56] J. K. Ahn *et al.* [E391a Collaboration], Phys. Rev. D **81**, 072004 (2010) [arXiv:0911.4789 [hep-ex]].
- [57] A. Freitas, JHEP **1404**, 070 (2014) [arXiv:1401.2447 [hep-ph]].
- [58] M. Aaboud *et al.* [ATLAS Collaboration], Phys. Lett. B **761**, 372 (2016) [arXiv:1607.03669 [hep-ex]].
- [59] M. Fairbairn, J. Heal, F. Kahlhoefer and P. Tunney, JHEP **1609**, 018 (2016) [arXiv:1605.07940 [hep-ph]].
- [60] G. Aad *et al.* [ATLAS Collaboration], Phys. Rev. D **91**, no.5, 052007 (2015) doi:10.1103/PhysRevD.91.052007 [arXiv:1407.1376 [hep-ex]].
- [61] G. Aad *et al.* [ATLAS Collaboration], Phys. Lett. B **754**, 302 (2016) [arXiv:1512.01530 [hep-ex]].
- [62] V. Khachatryan *et al.* [CMS Collaboration], Phys. Rev. D **91**, no.5, 052009 (2015) [arXiv:1501.04198 [hep-ex]].
- [63] V. Khachatryan *et al.* [CMS Collaboration], Phys. Rev. Lett. **116**, no.7, 071801 (2016) [arXiv:1512.01224 [hep-ex]].
- [64] D. Barducci, G. Belanger, J. Bernon, F. Boudjema, J. Da Silva, S. Kraml, U. Laa and A. Pukhov, arXiv:1606.03834 [hep-ph].
- [65] V. M. Abazov *et al.* [D0 Collaboration], Phys. Rev. D **87**, no. 5, 052011 (2013) [arXiv:1211.2466 [hep-ex]].
- [66] G. Aad *et al.* [ATLAS Collaboration], JHEP **1501**, 068 (2015) [arXiv:1411.6795 [hep-ex]].
- [67] P. A. R. Ade *et al.* [Planck Collaboration], Astron. Astrophys. **594**, A13 (2016) [arXiv:1502.01589 [astro-ph.CO]].
- [68] D. S. Akerib *et al.* [LUX Collaboration], Phys. Rev. Lett. **112**, 091303 (2014) [arXiv:1310.8214 [astro-ph.CO]].
- [69] D. S. Akerib *et al.* [LUX Collaboration], Phys. Rev. Lett. **116**, no.16, 161301 (2016) [arXiv:1512.03506 [astro-ph.CO]].
- [70] C. Amole *et al.* [PICO Collaboration], Phys. Rev. D **93**, no.5, 052014 (2016) [arXiv:1510.07754 [hep-ex]].

- [71] M. G. Aartsen *et al.* [IceCube Collaboration], JCAP **1604**, no.04, 022 (2016) [arXiv:1601.00653 [hep-ph]].
- [72] A. Semenov, Comput. Phys. Commun. **180**, 431 (2009) [arXiv:0805.0555 [hep-ph]].
- [73] A. Semenov, arXiv:1005.1909 [hep-ph].
- [74] A. Semenov, Comput. Phys. Commun. **201**, 167 (2016) [arXiv:1412.5016 [physics.comp-ph]].
- [75] A. Belyaev, N. D. Christensen and A. Pukhov, Comput. Phys. Commun. **184**, 1729 (2013) [arXiv:1207.6082 [hep-ph]].
- [76] G. Bélanger, F. Boudjema, A. Pukhov and A. Semenov, Comput. Phys. Commun. **192**, 322 (2015) [arXiv:1407.6129 [hep-ph]].
- [77] J. Da Silva, arXiv:1312.0257 [hep-ph].
- [78] U. Ellwanger and C. Hugonie, Comput. Phys. Commun. **175**, 290 (2006) [hep-ph/0508022].
- [79] F. Domingo, Eur. Phys. J. C **76**, no. 8, 452 (2016) doi:10.1140/epjc/s10052-016-4298-z [arXiv:1512.02091 [hep-ph]].
- [80] P. Bechtle, O. Brein, S. Heinemeyer, O. Stl, T. Stefaniak, G. Weiglein and K. E. Williams, Eur. Phys. J. C **74**, no.3, 2693 (2014) [arXiv:1311.0055 [hep-ph]].
- [81] S. Kraml, S. Kulkarni, U. Laa, A. Lessa, W. Magerl, D. Proschofsky-Spindler and W. Waltenberger, Eur. Phys. J. C **74**, 2868 (2014) [arXiv:1312.4175 [hep-ph]].
- [82] S. Kraml *et al.*, arXiv:1412.1745 [hep-ph].
- [83] E. Aprile *et al.* [XENON Collaboration], JCAP **1604**, no.04, 027 (2016) [arXiv:1512.07501 [physics.ins-det]].
- [84] G. Blanger, J. Da Silva, T. Perrillat-Bottonet and A. Pukhov, JCAP **1512**, no. 12, 036 (2015) [arXiv:1507.07987 [hep-ph]].